# Combined Theoretical and Experimental Investigation of Airfoil Encountering Transverse Gust

Yi Tsung Lee\*
North Carolina State University, Raleigh, NC 27695-7910, USA

Antonios Gementzopoulos<sup>†</sup> *University of Maryland, College Park, MD 20740, USA* 

Nitin Chitrala<sup>‡</sup>
North Carolina State University, Raleigh, NC 27695-7910, USA

Arun Vishnu Suresh Babu<sup>§</sup>
University of North Carolina at Charlotte, Charlotte, NC 28223-0001, USA

Anya R. Jones<sup>¶</sup> University of Maryland, College Park, MD 20740, USA

Ashok Gopalarathnam 

North Carolina State University, Raleigh, NC 27695-7910, USA

We present results of an airfoil encountering transverse gusts using theoretical modeling using a modified discrete-vortex method, performed at NC State University, and experimental testing using a tow tank facility, performed at the University of Maryland. The theoretical framework is based on a 2D lumped vortex element (LVE) method to model the unsteady flow resulting from an airfoil encountering a transverse gust. An important feature of the model is an approach to predict intermittent LEV shedding using the leading edge suction parameter (LESP), which is a measure of the suction at the leading edge, and is affected by contributions from airfoil kinematics, discrete vortices in the flowfield, and the gust during the gust encounter. With this theoretical unsteady model capable of predicting LEV shedding, we conducted several simulations of an airfoil encountering different transverse gusts and compared them with results from experiments in a tow tank. The results show that the model-predicted flowfield development is in good qualitative agreement with experiments, including the LEV formation. However, the model over-predicts lift history compared to experiments. It was hypothesized that the three-dimensional (finite-wing) effects might be the primary cause of this lift discrepancy. To test this hypothesis, a series of experiments with wings having different aspect ratios were conducted. The 2D theoretical results were corrected for aspect-ratio effects using Helmbold's equation. The lift histories predicted by the theory (with aspect-ratio corrections) show significantly improved comparison to the experimental results for all aspect ratios, which indicates the importance of taking finite-wing effects into consideration in both experimental and theoretical studies of transverse gust encounter.

#### **Nomenclature**

x chordwise coordinate

<sup>\*</sup>Ph.D. student, Department of Mechanical and Aerospace Engineering, ylee26@ncsu.edu, Student Member, AIAA

<sup>&</sup>lt;sup>†</sup>Ph.D. student, Department of Aerospace Engineering, ageme@umd.edu, Student Member, AIAA

<sup>&</sup>lt;sup>‡</sup>Undergraduate Student, Department of Mechanical and Aerospace Engineering, nachitra@ncsu.edu

<sup>§</sup>Assistant Professor, Box 7910, asures10@uncc.edu, Member, AIAA

<sup>¶</sup>Professor, arjones@umd.edu, Associate Fellow, AIAA

Professor, Box 7910, agopalar@ncsu.edu, Associate Fellow, AIAA

 $\theta$  chordwise angular coordinate

lpha airfoil pitch angle  $\phi$  velocity potential  $\Gamma$  vortex core strength  $U_{\infty}$  freestream velocity

*u* velocity in horizontal(x) direction*w* velocity in vertical(z) direction

 $w_g$  gust velocity W downwash velocity  $t^*$  non dimensional time

BV bound vortexFV free vortex

# I. Introduction

Unsteady aerodynamics is the study of motion through a flow field whose properties change with time. Studying unsteady aerodynamics is necessary to understand and model time-dependent phenomena such as flutter (Berci [1]), vortex-shedding (Shukla et al. [2]), gust-foil interactions (Medina et al. [3]), to name a few. These flow conditions present problems to flight stability, as most instabilities are caused by sudden changes in flow properties. Among unstable flow phenomena, one that is heavily considered when analyzing the lift of a wing is leading-edge vortex (LEV) shedding. LEV shedding was first discovered in the late 1900s when a number of studies were done by biologists to uncover the secrets of natural flight (Ellington [4], Dickinson et al. [5], Ellington et al. [6], and Pullin et al. [7]). They discovered a flow structure that was the result of the unsteady motions of an insect wing, which was later termed an LEV. They determined that immediately after the LEV was shed, there was a subsequent increase in lift which decreased as the LEV advected away from the wing surface [8]. A similar phenomenon is also observed when an airplane wing is exposed to a field of gust.

Broadly, gust refers to a sudden change in velocity within the flow field. The earliest gust research dates back to the 1930s when Küssner [9] determined that transverse gusts caused the highest wing stresses compared to gusts acting in other directions. Experimentally, Küssner attributed the effect of this vertical gust to a change in the angle of attack, recording airplane wing deflection during stormy weather. During flight, entering a region of gust momentarily alters the airplane angle of attack, which can cause flight-path deviations and additional loading. The strength of the gust is typically defined with a parameter called gust ratio, GR, which is defined as the maximum gust velocity relative to the free stream velocity. This ratio can help quantify the severity of the effect of gust, which can span from slight discomfort to severe structural damage [10].

Following Küssner's observations, an increased emphasis was placed on understanding the effects of transverse gusts in later research, and some other on mitigating the lift overshoot due to the gust, such as the work by Herrmann et al. [11]. In recent research, there are two main gust profiles that have been studied: transverse sine-squared gust encounters and top-hat transverse gust encounters. Corkery et al. [12] used a pump and ducting system to create a flow field through which a wing model is towed. From this, they were able to simulate a top-hat gust encounter. Particle image velocimetry (PIV) measurements of the wing encountering such gusts showed the formation of a strong LEV and significant deformation of the shear layers at the gust boundaries. Andreu-Angulo et al. [13] compared the two profiles, finding large discrepancies between the force measurements. They found that this was likely caused by differences in the shear layer distribution of the two profiles. They further reiterated the importance of LEV shedding on lift, finding that the top-hat gust profile had a significantly higher level of circulation shed within the gust region due to the formation of the strong LEV. Recently, more research has been dedicated to the goal of mitigating the gust effect. Sedky et al. [14] present three maneuvers which have been used in lift regulation as a means of mitigating gust effects. The first of the three maneuvers is to oppose the induced angle of attack from gust  $\alpha_{gust}$  with airfoil pitch angle  $\alpha$  such that the sum of the two equals to zero. This maneuver assumes fully attached flow and thus does not shed an LEV as shown in the experiments done by Corkery [12] and Andreu-Angulo [13]. The second maneuver is designed such that the total lift response from the superposition of Wagner and Küssner's lift response functions sums to zero. Wagner [15] gives the lift response as a function of angle of attack whereas Küssner gives the lift response of a wing exposed to gust. This maneuver assumes fully attached flows at small angles of attack and thus is ineffective at mitigating strong gusts. The third maneuver uses an unsteady Discrete Vortex Model (DVM) [16] to obtain a wing's pitch kinematics. The velocity

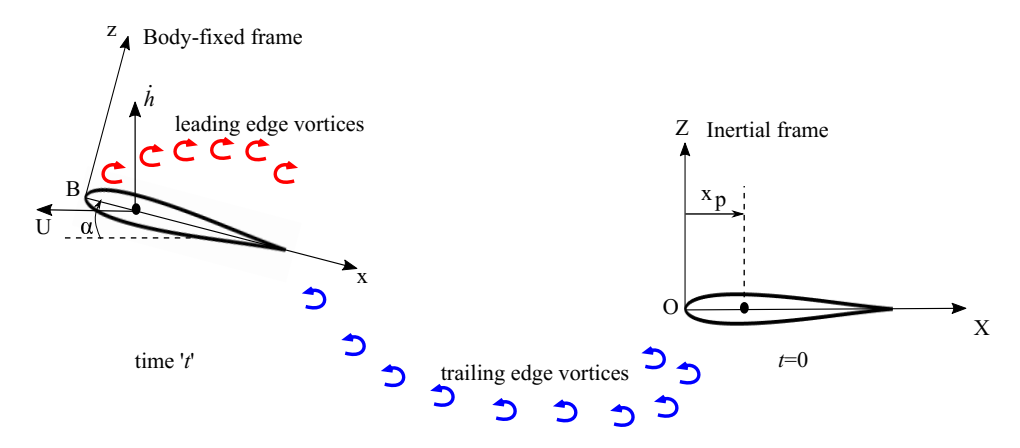


Fig. 1 Illustration of the airfoil kinematics and the discrete vortices shed from it, along with the variables used in the unsteady aerodynamic model

field, including the gust, is predetermined and is imposed on the wing's control points, bound vortices, and shed vortices within the flow field. LEV and Trailing-Edge Vortex (TEV) shedding are enforced by the Kutta condition at both edges of the airfoil.

This paper will use a low-order modeling approach to study a wing entering and exiting a region of gust. The use of low-order modeling in unsteady aerodynamics has gained a lot of traction in recent years, leading to a number of different models capable of analyzing various flow phenomena. Low-order modeling methods are designed to reduce the time and cost needed to analyze unsteady aerodynamics using computational fluid dynamics (CFD) or experimental procedures by capturing key unsteady flow phenomena without too complex of calculations. To develop such a model, the challenge is to rapidly and accurately capture one of the most important unsteady flow physics: leading edge vortex shedding, and its effect on an airfoil. There has been a lot of attempts on achieving the goal, and among these efforts, the concept of leading-edge suction force, which keeps the flow attached until the suction can no longer support the flow attachment, has gained a lot of interest. Ramesh et al. [17] first proposed a parameter called leading edge suction parameter (LESP) and used it as a parameter within unsteady thin airfoil theory to create a mechanism for predicting LEV shedding initialization and termination. It states that an airfoil at a Reynolds number will have a critical LESP value that is largely independent of motion kinematics. As long as the instantaneous LESP is less than the critical value, the leading-edge flow stays attached. When the LESP exceeds the critical value, LEV shedding starts, resulting in the growth of the LEV structure. The same concept has been inherited by Narsipur et al. [18, 19] with a Lumped-Vortex Element (LVE) model as the basis for trailing edge separation prediction. A more detailed study on leading edge suction force in CFD has been done in the work of Narsipur et al. [20] and experimentally by Saini et al. [21, 22]. The improvement and modification to increase the low order model's capability has also been done in the work of SureshBabu [23] and Lee et al. [24], where model reduction and a state variable form to couple with structure dynamic equations are investigated. In this paper, we follow the work of Narsipur et al. [19] to construct our low-order model and add a region of top-hat profile transverse gust to simulate the gust encounter problem. To assess the accuracy of this low-order model with an added field of gust, experiments similar to the work in Sedky et al. [14] are conducted and used as the reference. The effect of the gust ratios and wing aspect ratios are studied by comparing the lift history and the flow field data from the low-order model and experiments.

The paper will be organized as follows: Sec. II will introduce the basic LVE method and the LESP for the LEV shedding mechanism along with gust implementation to the solver. Sec.III will introduce the experimental setup and parameters used in the experiments. The following Sec. IV demonstrates the results of the gust profile, lift prediction, and flow field velocity and vorticity distribution compared to experimental results. The effect of the gust ratio and the wing aspect ratio are also discussed in this section. Finally, in Sec. V, we summarize the current conclusion from our theoretical and experimental work.

# II. Theory

The schematic representation in figure 1 shows an airfoil of chord c undergoing arbitrary prescribed pitching and heaving kinematics. The kinematic state of the airfoil is defined by the pitch angle,  $\alpha$ , the heave position, h, and the

respective velocities,  $\dot{\alpha}$  and  $\dot{h}$ . The pivot point, located at a distance  $x_p$  aft of the leading edge, denotes the center of rotation of the airfoil. Also shown is a body-fixed frame, Bxz, with the origin coinciding with the leading edge of the airfoil and the x and z axes extending in the chord-wise and chord-normal directions, respectively. The wake of the airfoil consists of discrete LEVs and TEVs shed from either edge of the airfoil in the previous time steps.

### A. Lumped Vortex Element model and the Unsteady Thin Airfoil Theory

The Lumped Vortex Element (LVE) method and Thin Airfoil Theory assume that an airfoil can be represented by several bound vortex elements concentrated on points along the camberline of the airfoil. The airfoil can be separated into several panels, with each bound vortex at the quarter-chord position of the panel as a discrete bound vortex element, and a control point at the three-quarter-chord position of the panel. The concentrated bound vortex strength on each panel is presented by  $\Gamma$ . Based on the Unsteady Thin Airfoil Theory, at any time instant, the zero-normal-flow condition needs to be fulfilled following the equations below:

$$\left(\nabla\phi_B + \nabla\phi_w + \vec{U}_0 - \vec{U}_{rel} - \dot{\alpha} \times \vec{r}\right) \cdot \vec{n} = 0 \tag{1}$$

In this equation,  $\nabla \phi_B$  is the velocity induced due to the velocity potential from bound vortex elements, while  $\nabla \phi_w$  is the velocity induced due to all the free vortices. The  $\vec{U_0}$  is the free stream velocity vector,  $\vec{U}_{rel}$  is the translational velocity of the airfoil, and  $\dot{\alpha} \times \vec{r}$  is the velocity induced due to the airfoil pitching motion, where  $\dot{\alpha}$  is the pitch angular velocity and  $\vec{r}$  is the position vector of a point on the airfoil relative to the pivot point. This equation will be applied on all the N control points on the camberline and provide N equations to solve the corresponding unknowns, which are the instantaneous bound vortex strengths along the camberline. As a result, the equation is typically separated into two sides as follows:

$$\nabla \phi_B \cdot \vec{n} = -\left(\nabla \phi_w + \vec{U}_0 - \vec{U}_{rel} - \dot{\alpha} \times \vec{r}\right) \cdot \vec{n} = -Wn \tag{2}$$

This can be realized as the self-induced velocity on the control points normal to the panel due to the bound vortices having to be balanced by the right-hand side, -Wn, which is the contribution from wake-induced velocity, free stream, and motion resulting velocity normal to the panel. The sum of these velocities normal to the *i*th panel is referred to as downwash, and can be separated as follows:

$$Wn_i = \vec{W}_i \cdot \vec{n}_i = (\vec{W}_i^{U_0} + \vec{W}_i^{U_{rel}} + \vec{W}_i^{\dot{\alpha}} + \vec{W}_i^{FV}) \cdot \vec{n}_i$$
(3)

This shows that there are four parts inside the downwash: free stream  $\vec{W}_i^{U_0}$ , airfoil translation motion  $\vec{W}_i^{Crel}$ , airfoil pitching motion  $\vec{W}_i^{\dot{\alpha}}$  and free vortex-induced velocity  $\vec{W}_i^{FV}$ . Induced velocity due to free vortex and bound vortex on any point can be calculated using the Biot-Savart law at x and z direction as:

$$u_i = \frac{\Gamma_j}{2\pi r_{ij}^2} (z_i - z_j) \tag{4}$$

$$w_i = -\frac{\Gamma_j}{2\pi r_{ij}^2} (x_i - x_j) \tag{5}$$

$$r_{ij}^2 = \sqrt{((x_i - x_j)^2 + (z_I - z_j)^2)^2 + \delta v_{core}^4}$$
 (6)

This equation gives the induced velocity  $\vec{u}_i$  at position  $\vec{x}_i$  due to the vortex at  $\vec{x}_j$  with vortex strength  $\Gamma_j$ . The distance between the point i and point j is defined using Equation (6), with a special term  $\delta v_{core}^4$ . The value of  $\delta$  will be zero when the distance is calculated between the control points and bound vortex points since the distance is usually a fixed value, while  $\delta$  will be unity when the distance equation is used for calculating induced velocity from free vortices. This term is designed to prevent the effect of the free vortex being too close to any bound vortex or any other free vortex and creating an unrealistically large induced velocity. Based on the work of Leonard [25], the vortex core distance  $v_{core}$  is defined as follows:

$$v_{core} = 1.3c\Delta t^*,\tag{7}$$

where  $\Delta t^*$  is the non-dimensional time step. The self-induced velocity term on the left-hand side of Equation (2) can be expressed at the control point of each panel. The unit induced velocity on control point *i* due to the bound vortex on

panel j is represented as an influence coefficient  $a_{ij}$  with the strength  $\Gamma_i$ :

$$a_{ij} = \left(\frac{1}{2\pi r_{ij}^2} (z_i - z_j), -\frac{1}{2\pi r_{ij}^2} (x_i - x_J)\right) \cdot \vec{n}_i \tag{8}$$

For panel i, the total induced velocity normal to the panel  $q_i$  from all the N bound vortex elements can be written as follows:

$$q_i = a_{i1}\Gamma_1 + a_{i2}\Gamma_2 + \dots + a_{iN}\Gamma_N \tag{9}$$

The balance between the self-induced velocity and the right-hand side is written as an influence matrix equation as follows, which is valid at any time instant and can be used in both steady and unsteady simulation.

$$\begin{bmatrix} a_{11} & a_{12} & \cdots & a_{1N} \\ a_{21} & a_{22} & \cdots & a_{2N} \\ \vdots & \vdots & \ddots & \vdots \\ a_{N1} & a_{N2} & \cdots & a_{NN} \end{bmatrix} \begin{bmatrix} \Gamma_1 \\ \Gamma_2 \\ \vdots \\ \Gamma_N \end{bmatrix} = \begin{bmatrix} -Wn_1 \\ -Wn_2 \\ \vdots \\ -Wn_N \end{bmatrix}$$
(10)

## B. LESP and vortex shedding

Continuous vortex shedding from the trailing edge and in some cases from the leading edge is the most important phenomenon responsible for the aerodynamic unsteadiness. To expand the usual influence matrix equation for vortex shedding, a new TEV and a new LEV will be released into the field, with the positions defined following Narsipur's work[19]. To handle these additional unknowns, the first new equation to help solve the bound vortex strength and the new TEV/LEV strength will be the Kelvin condition, which is as follows:

$$\sum \Gamma_b(t - \Delta t) = \sum \Gamma_b(t) + \Gamma_{TEV} + \Gamma_{LEV}$$
(11)

At the start of every step, we assume that there is no LEV shedding but only TEV shedding resulting in  $\Gamma_{LEV} = 0$ , which gives only N + 1 unknowns with now N + 1 equations as follows:

$$\begin{bmatrix} a_{11} & a_{12} & \cdots & a_{1N} & a_{1tev} \\ a_{21} & a_{22} & \cdots & a_{2N} & a_{2tev} \\ \cdots & \cdots & \cdots & \cdots & \cdots \\ a_{N1} & a_{N2} & \cdots & a_{NN} & a_{Ntev} \\ 1 & 1 & \cdots & 1 & 1 \end{bmatrix} \begin{bmatrix} \Gamma_1 \\ \Gamma_2 \\ \cdots \\ \Gamma_N \\ \Gamma_{TEV} \end{bmatrix} = \begin{bmatrix} -Wn_1 \\ -Wn_2 \\ \cdots \\ -Wn_N \\ \sum \Gamma_b(t - \Delta t) \end{bmatrix}$$
(12)

This equation can be used to solve the instantaneous bound vortex strength and the new TEV strength. To further determine if LEV shedding should be activated at the current step, we introduce a parameter called the Leading Edge Suction Parameter (LESP) from the work of Ramesh et al. [17]. LESP is a parameter representing how strong the suction is at the leading edge of an airfoil, and is a parameter governed by the strength of the first bound vortex based on the work of Aggarwal [26] using the following definition:

$$LESP(t) = \frac{1.13(\Gamma_1(t))}{U_{\infty}(t)c\left[cos^{-1}(1-\frac{2l}{c}) + sin(cos^{-1}(1-\frac{2l}{c}))\right]}$$
(13)

The idea of LESP is that for each airfoil at each Reynolds number, there is a maximum suction force it can support, which is defined as  $LESP_{crit}$ . When the instantaneous |LESP| surpasses the  $LESP_{crit}$ , LEV shedding will be started, indicating that the airfoil can no longer support enough suction at the leading edge to keep the flow attached. More details on LESP can be found in previous work. [17, 20, 27] When LEV shedding is active, the LESP will be maintained at the  $LESP_{crit}$ , which means that the first bound vortex strength will now be determined. Using this information, whenever the pure TEV shedding calculation is finished and the result of  $\Gamma_1$  contributes to a larger |LESP| than the  $LESP_{crit}$ , the LEV shedding will be activated and we will have a new influence matrix equation to solve:

$$\begin{bmatrix} a_{12} & \cdots & a_{1N} & a_{1tev} & a_{1lev} \\ a_{22} & \cdots & a_{2N} & a_{2tev} & a_{2lev} \\ \cdots & \cdots & \cdots & \cdots & \cdots \\ a_{N2} & \cdots & a_{NN} & a_{Ntev} & a_{Nlev} \\ 1 & \cdots & 1 & 1 & 1 \end{bmatrix} \begin{bmatrix} \Gamma_2 \\ \cdots \\ \Gamma_{N} \\ \Gamma_{TEV} \\ \Gamma_{LEV} \end{bmatrix} = \begin{bmatrix} -Wn_1 \\ -Wn_2 \\ \cdots \\ -Wn_N \\ \sum \Gamma_b(t - \Delta t) \end{bmatrix} - \begin{bmatrix} a_{11} \\ a_{21} \\ \cdots \\ a_{N1} \\ 1 \end{bmatrix} \Gamma_{1,crit}$$

$$(14)$$

Where the  $\Gamma_{1,crit}$  is the value that will result in  $LESP = LESP_{crit}$ . With this influence matrix equation, the solver can solve the strength of newly shed TEV/LEV and the bound vortex strength simultaneously.

Once the strengths of bound vortices and free vortices are determined, each free vortex is convected using its induced velocity, which comes from the effect of induced velocity due to free stream, bound vortices, and all other free vortices as follows:

$$\vec{u}_{FV} = \vec{u}_{\infty} + \vec{u}_{ind,BV} + \vec{u}_{ind,FV} \tag{15}$$

### C. Modeling the Gust Effect

To simulate the gust effect, the basic theory is that when any point of interest such as control points or free vortex positions is within the gust region, the velocity calculation will need to include the effect of gust. In the current work, we create a specific gust field function that can calculate the corresponding gust velocity at any point of interest. We add the contribution from the gust field function to zero normal flow boundary conditions and the calculation of the velocity of the free vortices. The first modification is that the right-hand side of the influence matrix equation of each panel will now be:

$$Wn_i = \vec{W}_i \cdot \vec{n}_i = (\vec{W}_i^{U_0} + \vec{W}_i^{U_{rel}} + \vec{W}_i^{\dot{\alpha}} + \vec{W}_i^{FV} + \vec{w}_g(\vec{x}_i)) \cdot \vec{n}_i)$$
(16)

where  $\vec{w}_g(\vec{x}_i)$  is the local gust velocity vector at position  $x_i$ . The second modification will be that the velocity of all the free vortices needs to account for this additional gust velocity:

$$\vec{u}_{FV} = \vec{u}_{\infty} + \vec{u}_{ind,BV} + \vec{u}_{ind,FV} + \vec{w}_{\varrho} \tag{17}$$

This modification shows that the gust directly affects the corresponding bound vortex strength when the airfoil is within the gust region, so the load distribution and whether an LEV is shed or not are both affected. The other impact is that the gust will directly change how the free vortices move in the flow field due to direct velocity changes.

## **D. Load Prediction**

The current method calculates the gust effect on how the free vortices move and the corresponding bound vortex strength distribution. To extend these to an aerodynamic load, unsteady Bernoulli equations can be used to calculate the pressure difference, based on the work of SureshBabu et al. [23]:

$$\Delta p(x) = \rho \left[ \left( U \cos \theta + \dot{h} \sin \theta + u_{ind}(x) \right) \gamma(x) + \frac{\partial}{\partial t} \int_{x'=0}^{x} \gamma(x') dx' + \dot{\Gamma}_{lev} \right]$$
 (18)

This expression uses a continuous bound circulation distribution  $\gamma(x)$ , which can be modified for the current panel method with discrete bound vortex strengths. Notice that the first part of the contribution comes from the downwash velocity tangential to the panel, so the gust-induced velocity should also be taken into account. As a result, the final local pressure difference at panel i is then defined by

$$\Delta p_i = \rho \left( \vec{U}_0 - \vec{U}_{rel} - \dot{\alpha} \times \vec{r} + \vec{u}_w + \vec{w}_g \right) \cdot \vec{\tau}_i \frac{\Gamma_i}{l_i} + \frac{\partial}{\partial t} \sum_{k=1}^{k=i} \Gamma_k + \dot{\Gamma}_{lev}$$
 (19)

Here,  $\Gamma_i$  refers to the bound vortex strength of the *i*th panel,  $l_i$  refers to the length of the *i*th panel,  $\vec{\tau}_i$  refers to the tangential vector of the panel and  $\vec{u}_w$  refers to the induced velocity vector due to all the free vortices. In (18) and (19), the third term explicitly takes into account the effect of circulation production due to LEV shedding on the unsteady loads of the airfoil. The first term is the circulatory term and relies on the velocity tangential to the panel and the bound vortex sheet strength while the second term is referred to as the apparent mass term.

The normal and suction force coefficients can be derived by summing the pressure difference and is given as:

$$C_N = 2 \frac{\sum_{i=1}^N \Delta p_i l_i}{\rho U_\infty^2 c} \tag{20}$$

$$C_S = 2\pi L E S P^2(t) \tag{21}$$

Using the normal and the suction force coefficients, the lift and drag coefficients can be evaluated as:

$$C_L = C_N \cos \alpha + C_S \sin \alpha \tag{22}$$

$$C_D = C_N \sin \alpha - C_S \cos \alpha \tag{23}$$

The moment coefficient can be calculated using the equation,

$$C_{M} = -2 \frac{\sum_{i=1}^{N} \Delta p_{i} l_{i} (x_{i} - x_{pivot})}{\rho U_{\infty}^{2} c^{2}}$$
 (24)

## E. Finite Wing Correction

We hypothesize that the tip vortex in the experiment will cause lift reduction, and will be strongly related to the aspect ratio of the wing. To better compare the model with the experimental data, we apply a simple finite wing correction to the final lift results calculated from the low-order model. In this work, Helmbold's equation (equation 25) [28] is used to take into account the wing aspect ratio effect. Helmbold's equation calculates the corresponding lift curve slope *a* for a low-aspect-ratio straight wing.

$$a = \frac{a_0}{\sqrt{1 + [a_0/(\pi AR)]^2 + a_0/(\pi AR)}}$$
 (25)

In our experiments and the simulations, all the wings are pure flat plate meaning that the lift coefficient  $C_L$  starts at 0 at 0 degree angle of attack. This means that the ratio between corrected a and the two-dimensional lift curve slope  $a_0$  can be used to scale the lift from the two-dimensional simulation in order to better represent the actual lift of a three-dimensional wing. The corrected  $C_L$  is shown in equation 26.

$$C_L = C_{L,2D} \frac{a}{a_0} \tag{26}$$

# III. Experimental Methodology

Experiments are carried out in The University of Maryland (UMD) free surface water towing tank shown in figure 2. The tank dimensions are 7 m long, 1.5 m wide, and 1 m deep. The tank is equipped with a 4-degree-of-freedom model motion system, allowing for streamwise, streamnormal, and pitching motions. The freestream is created by towing the wing through the tank, and a transverse gust is created via a planar jet flow. Four carbon-fiber flat-plate half-wings with 8%-thick sections, a chord of 3 in and physical spans of 3, 6, 9, and 12 in of varying spans are tested at gust ratios of 0.4, 0.5, and 0.6, and at a Reynolds number of 10,000. A splitter plate is used on one side to act as a symmetry plane, resulting in effective full-wing aspect ratios of 2, 4, 6, and 8. In the remainder of this paper, "aspect ratio" will refer to this full-wing effective aspect ratio. An ATI Mini-40 force/torque sensor is used to measure the loads on the wings at 1 kHz. The force measurements were filtered at a cutoff frequency of 5 Hz. Each experiment was repeated five times and all measurements were ensemble averaged over the five runs.

## **IV. Results**

The aerodynamic load from the experiment and the low-order method are compared and discussed in this section. The low-order simulation uses a small  $LESP_{crit} = 0.05$  to simulate a flat plate with a sharp leading edge where LEV shedding is easily triggered. In this section, the gust velocity, lift comparison between different gust ratios, and the lift comparison between wings with different aspect ratios will be discussed.

#### A. Gust Velocity Profile

Gust ratio, GR, is defined as the maximum gust velocity,  $w_{g,max}$ , relative to the free stream velocity  $U_{\infty}$  following the below definition:

$$GR = \frac{w_{g,max}}{U_{\infty}} \tag{27}$$

Although gust can be easily defined as two sections with zero gust and full gust individually, in the actual flow field there must be gust velocity gradient near the gust edges to smooth the velocity distribution to the neighboring free stream.

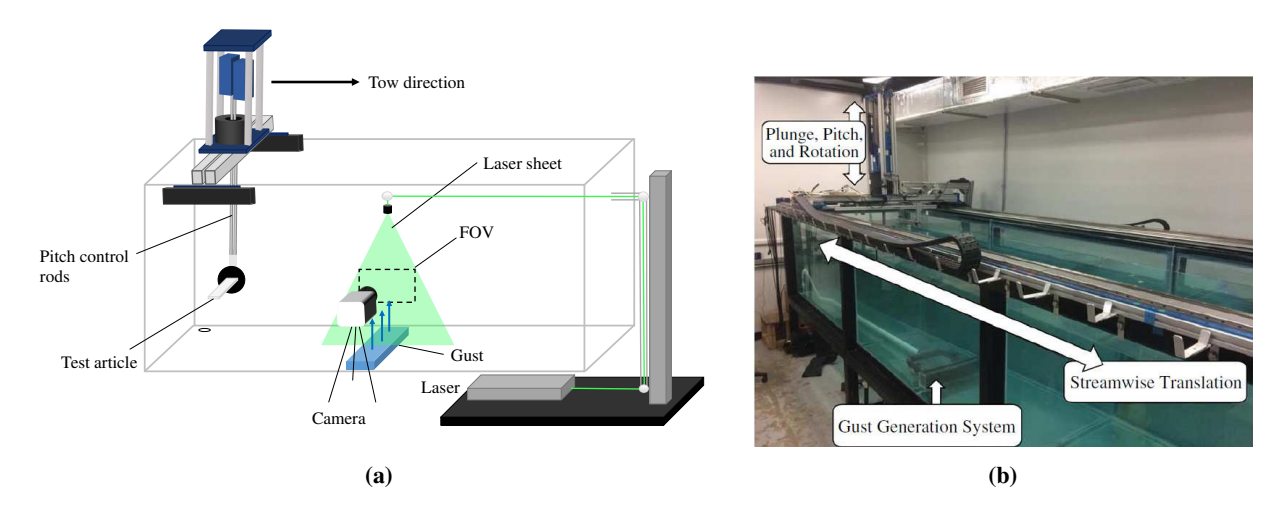


Fig. 2 Experimental apparatus at the University of Maryland water towing tank depicting (a) a schematic of the tow tank and the PIV configuration (b) the physical tow tank as well as the gust generator.

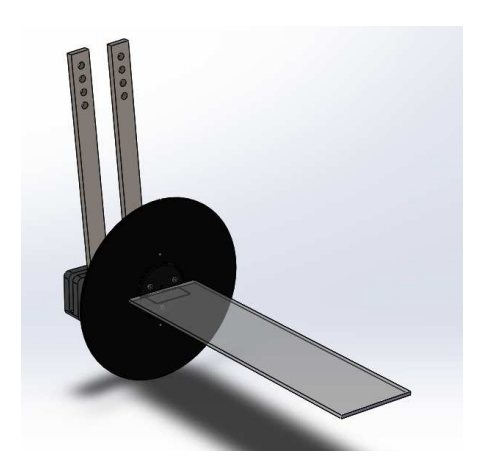


Fig. 3 The half-wing setup used in the experiments. A 6in endplate is used to isolate the effects of the attachment mechanism and the force balance on the flow.

Hence, we use a function inspired by the Eldredge pitch-up and return function[29], to create a gust velocity profile that smoothens the velocity distributions at the edge of the gust and creates a slope to merge the horizontal velocity to the free stream one. The gust velocity distribution can be defined using the following equation:

$$G(x) = \ln \left[ \frac{\cosh(a(x - x_1/)/c) \cosh(a(x - x_4/)/c)}{\cosh(a(x - x_2/)/c) \cosh(a(x - x_3/)/c)} \right]$$
(28)

with a being a smoothing parameter from Granlund et al.[30] to control the smoothing at four turning points of  $x_1$ ,  $x_2$ ,  $x_3$  and  $x_4$ . The final velocity profile is then defined by

$$w_g(x) = GR \cdot U_\infty \frac{G(x)}{\max(G(x))}$$
 (29)

The velocity profile used in the current study is shown in figure 4. By applying the Eldredge function to generate the gust velocity profile for the simulation, we successfully generate a curve that captures the velocity gradient at the edge of the gust, ensuring that the gust exposure time in the simulation is similar to that in the experiments.

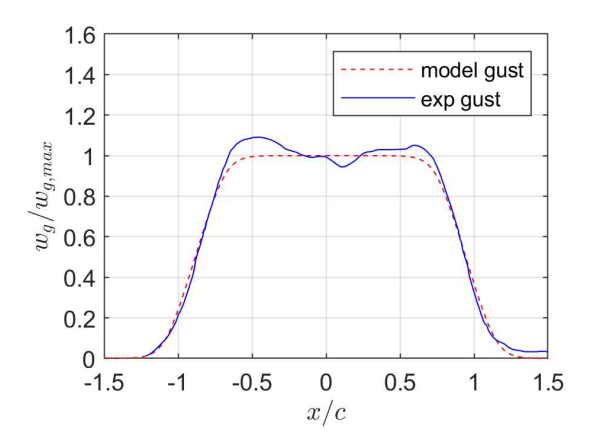


Fig. 4 Gust velocity profile comparison between the experimental measurement and the low-order model.

#### B. Effect of Gust Ratio on Lift

The lift from three different gust ratios GR = 0.4, 0.5 and 0.6 with wing aspect ratio AR = 4 in the experiments are plotted against the non-dimensional time  $t^*$  in figure 5, where the non-dimensional time can be defined as

$$t^* = tU_{\infty}/c \tag{30}$$

In the figure, the shaded region indicates the time period during which the flat plate is exposed to the transverse gust. Figure 5(a)(b) are the plots for the comparisons of the lift and normalized lift coefficient between the model and experiments, and (c)(d) are the plots when the model results are scaled using the finite wing correction. The figure shows that our low-order method in the current work can predict the lift increase when the airfoil enters the gust region and the corresponding lift drop when the airfoil departs from the gust region. The lift increases further when the strength of the gust is higher, but when normalized by the gust ratio, we can see that the curves collapse to the experimental results. It can be seen the low-order model also captures the overall lift behavior in good agreement with the experiments. The lift starts to increase once the leading edge of the airfoil enters the gust and keeps increasing until the time  $t^* = 1.7$ , which is approximately the time when the leading edge of the airfoil starts to move out of the full-strength gust region.

Although the low-order model captures this initial lift increase, it can easily be noticed that regardless of the gust ratio, all model-predicted lift is much higher than the experimental results. We hypothesize that this discrepancy is due to the absence of a tip vortex in the two-dimensional model. As shown in figure 5(c)(d), by applying the finite wing corrections based on Helmbold's equation using the wing aspect ratio in the experiment, all the lift prediction curves match better with experiments, indicating that the three-dimensional flow effect is important for the accuracy of the low-order model in such gust encounter simulation. Although the low-order model can predict the lift increase correctly, the prediction in the recovery part of the gust encounter, for example after  $t^* = 2.5$ , is not satisfactory. This may be due to the fact that although the model can predict the leading edge vortex shedding, some other viscous effect such as the flow separation is not modeled. Recent research from Narsipur et al. [19, 20] also shows drop in LESP during the LEV shedding process rather than maintaining it at the critical value. This change will affect the strength of the LEV shedding and may improve the lift prediction if we incorporate it in the current low-order model.

### C. Flow Field Prediction

The velocity and vorticity field from the experiment are used as the reference to compare the velocity field and shedding of discrete vortices from our low-order method. In figure 6, results from the experiment and the low-order model for gust ratio GR = 0.5 are presented, with the velocity being calculated on the airfoil frame. Although in the plot, our results only show the positions of leading-edge vortices (red) and trailing-edge vortices (blue) instead of a contour plot as the vorticity field, the discrete vortices do show a good match in positions to the points with strong vorticity in the experimental data. The results show that the model generally predicts an LEV shedding pattern and its corresponding velocity field in good agreement with the experimental data. This shows that the LEV shedding due to the contribution from the gust-induced velocity on an airfoil is successfully modeled by our solver. However, it is also worth noticing that LEV development from the model doesn't perfectly match the experiment in some later time steps

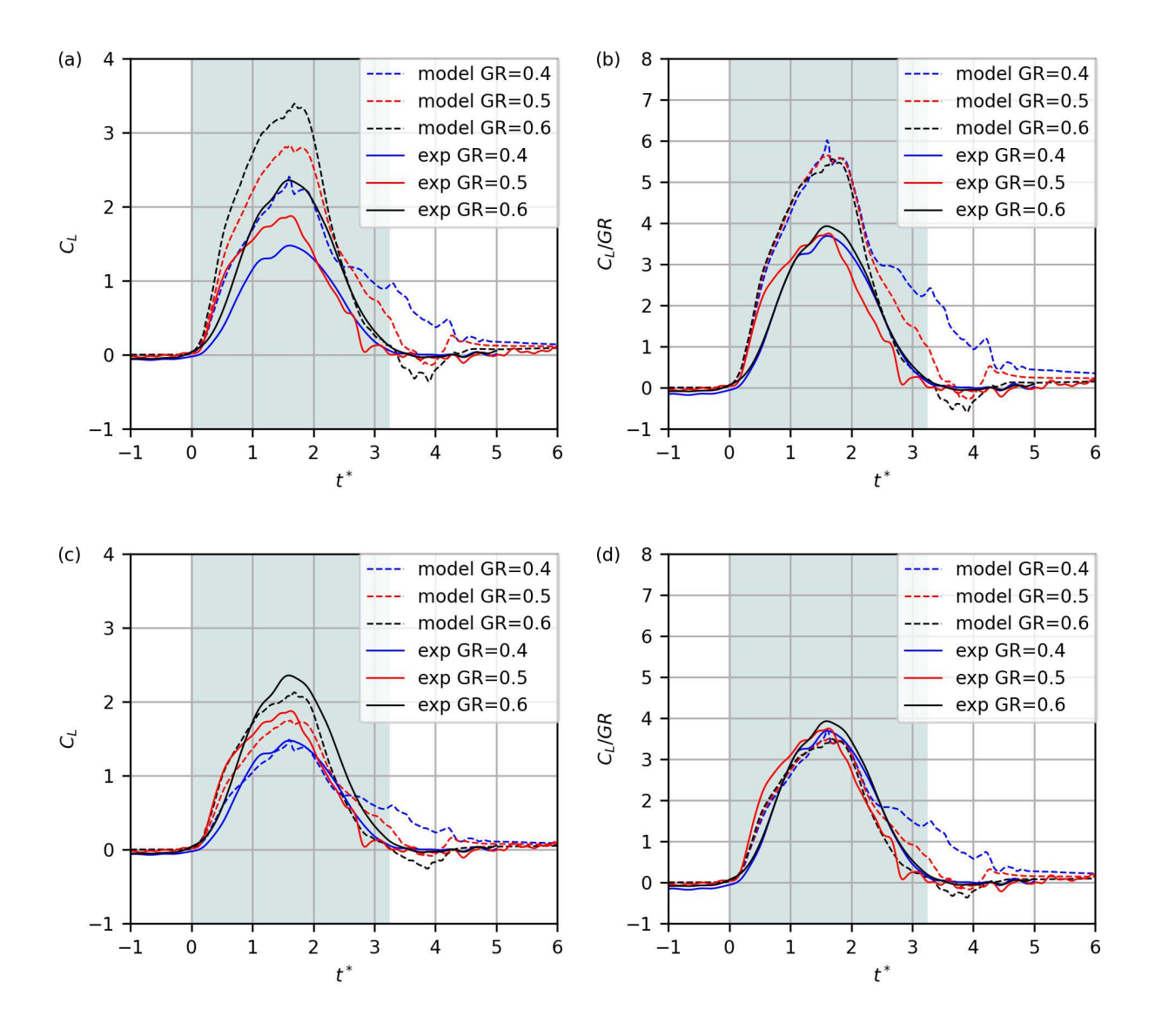


Fig. 5 Comparison of  $C_L$  between experiment and 2D low-order model: (a) direct comparison (b)  $C_L/GR$  comparison (c) low-order model with finite wing correction, AR = 4 (d)  $C_L/GR$  comparison to low-order model with finite wing correction, AR = 4.

such as after  $t^* = 2.0$ . The discrepancy between the discrete vortex pattern and the vorticity field may also be the cause of the lift difference between the model and the experimental results.

# D. Effect of Aspect Ratio on Lift

Improved accuracy of the low-order predictions while using the finite wing correction motivates further interest on the effect of the three-dimensional tip vortex on the lift history. The lift comparisons between the low-order model and the experiment of four wings are presented in this section. Two gust ratios GR = 0.4, and GR = 0.6 are studied for four wings with aspect ratios AR = 2,4,6, and 8. Figure 7(a) shows the comparison from the 2D low-order-model to the experiment, while Figure 7(b) shows the model with finite wing correction comparing to the experimental data. The experimental data itself shows how the wing aspect ratio affects lift increase differently during the gust encounter. The initial two-dimensional model over-predicts the lift significantly, but after the correction, the lift matches the experimental results much better. Similar observations can be made in figure 8, where cases with stronger gusts are

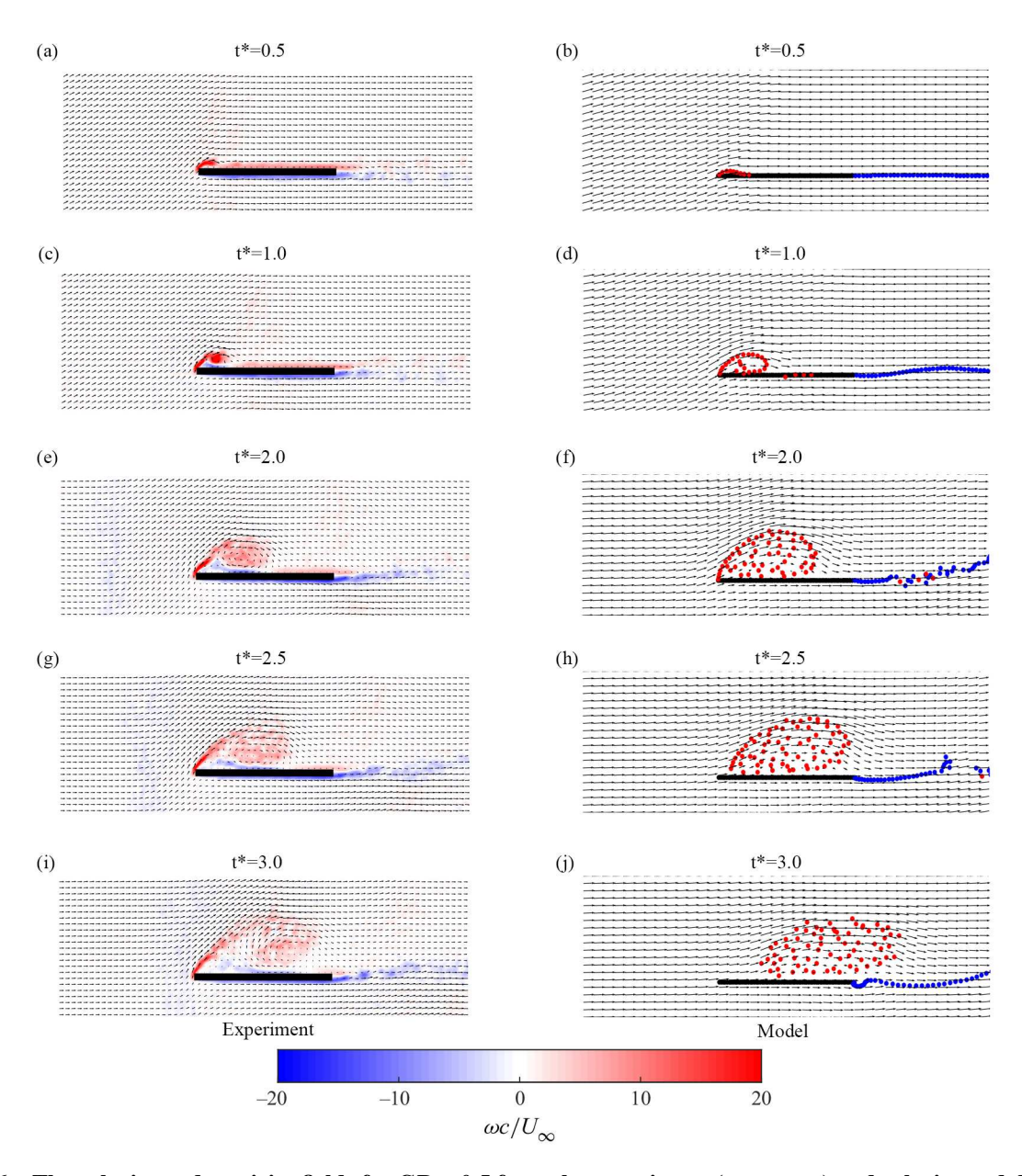


Fig. 6 The velocity and vorticity fields for GR = 0.5 from the experiment (a, c, e, g, i) and velocity and discrete-vortex positions from the low-order model (b, d, f, h, j) at several time instants.

compared. Although the finite wing corrections result in lift curves matching the experimental data much better than the pure 2D results, it can be seen that as the aspect ratio decreases, this simple correction will also scale down the lift too much. This indicates that the current correction is still far from perfect, and a more detailed study on how to properly address the three-dimensional tip vortex effect that reduces the lift increment due to the gust is needed. Furthermore, the lift prediction from the model when the airfoil moves away from the gust is always more noisy than the experimental data. This may be due to the termination of LEV shedding and its corresponding flow field interaction not being well captured by the model. Some other viscous effects not modeled in the simulation such as the trailing-edge separation and the viscous dissipation at the gust encounter might also contribute to the discrepancy between the experiment and the low-order model.

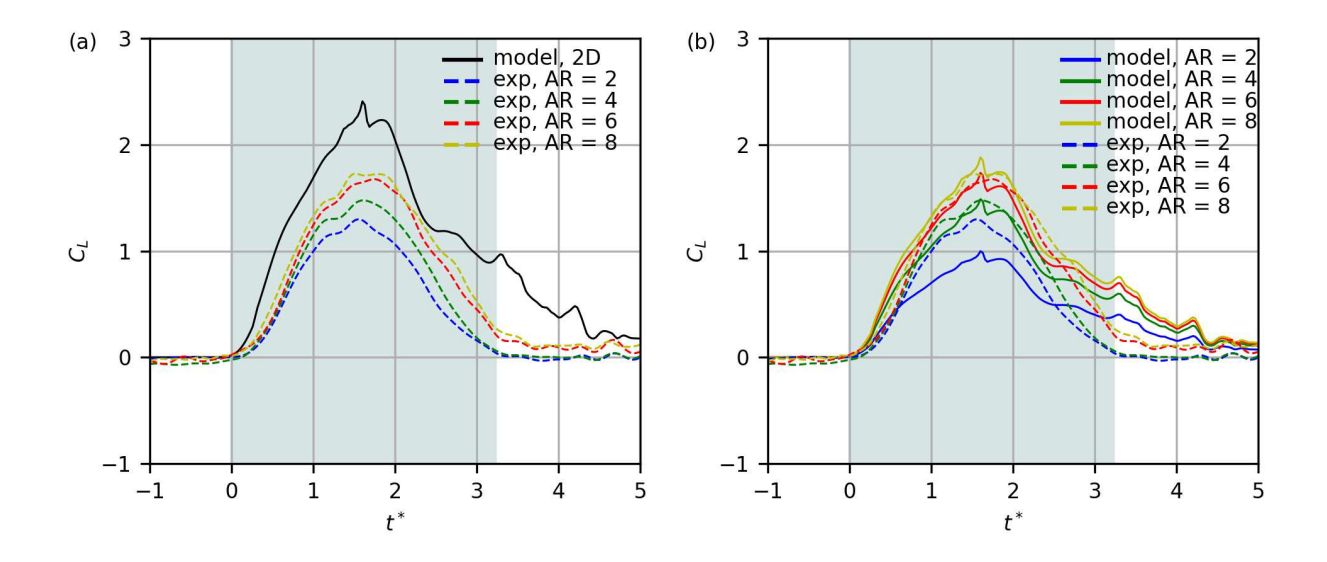


Fig. 7 The coefficient of lift  $C_L$  comparison for GR = 0.4: (a) experiment to 2D low-order model and (b) experiment to low-order model with finite wing correction.

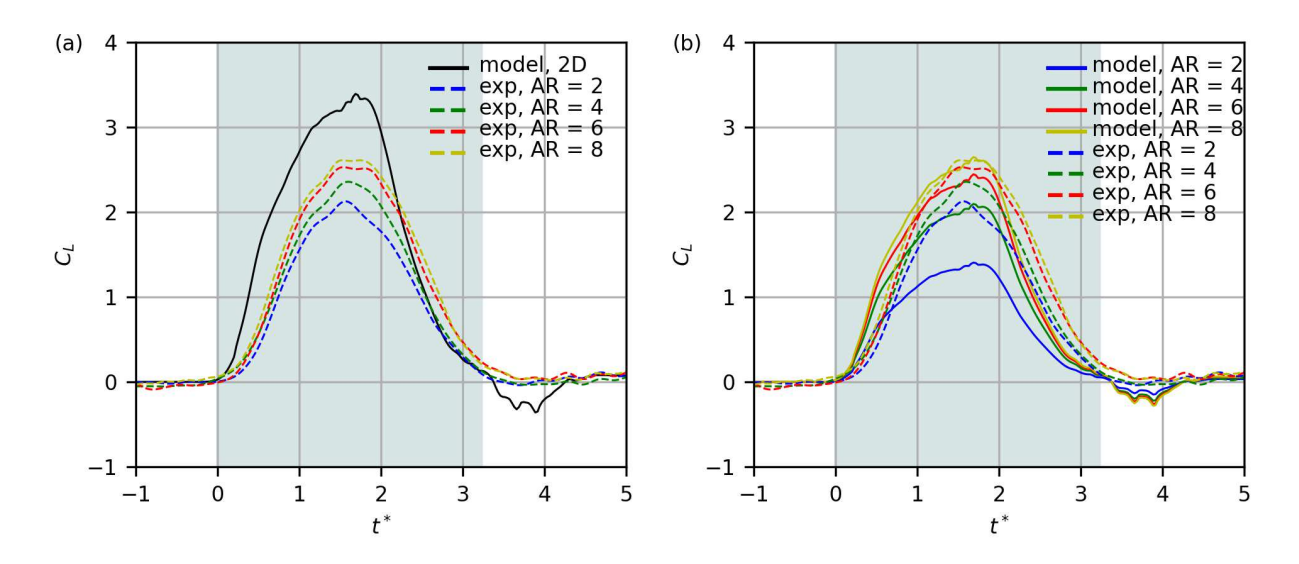


Fig. 8 The coefficient of lift  $C_L$  comparison for GR = 0.6: (a) experiment to 2D low-order model and (b) experiment to low-order model with finite wing correction.

# V. Conclusions

In this paper, we presented a low-order unsteady aerodynamic model capable of capturing the effect of a transverse gust encounter on the flow field and the lift of an airfoil. The model was built based on the work of Ramesh et al. [17] on predicting the initiation and termination of LEV shedding from unsteady airfoils in inviscid methods. Our model successfully predicts the LEV formation due to the transverse gust encounter in good agreement with experimental results. The lift prediction shows that lift increase is proportional to the strength of the gust, matching the observation from the experimental results. We compared the flow field prediction from the model with the experimental PIV data and observed that the LEV shedding was captured accurately by the model, which could explain the qualitative similarity of the lift history curve to the experimental results. However, the model also showed an obvious lift over-prediction, which we attributed to the finite wing effect in the experiments. To test the hypothesis, we adopted the correction using

Helmbold's equation to scale down the lift curve. The correction successfully brings down the lift from the model and results in better agreement with the experimental data.

Further experiments investigated the effect of the wing aspect ratio. The results from the model with finite wing correction and experimental data showed that the gust-induced lift increase is strongly related to the aspect ratio of the wing. The low-order model with the finite wing correction matched the experimental data much better than the pure two-dimensional simulation, indicating that the existence of tip vortices from a three-dimensional wing is also important in the lift increase during the transverse gust encounter. However, this simple correction developed from steady-state aerodynamics is limited to the current scenario, and might not be suitable for more complex situations such as the cases with unsteady motion of the wing. Some lift discrepancies between the model and the experiments also may be attributed to other viscous effects not being modeled in the current solver, and not just the three-dimensional effects. Overall, the observations indicate that in future experiments and simulations, the three-dimensional effect will need to be considered, and a more well-designed finite wing correction technique needs to be implemented in the low-order model.

# VI. Acknowledgment

The efforts of authors Lee and Gopalarathnam towards this research were supported in part by funding from the National Science Foundation under Award No. CMMI-2015983, managed by program officer Dr. Robert Landers. This support is gratefully acknowledged.

## References

- [1] Berci, M., "On Aerodynamic Models for Flutter Analysis: A Systematic Overview and Comparative Assessment," *Applied Mechanics*, Vol. 2, 2021. https://doi.org/10.3390/applmech2030029.
- [2] Shukla, R., and Eldredge, J. D., "An inviscid model for vortex shedding from a deforming body," *Theory of Computational Fluid Dynamics*, 2007. https://doi.org/10.1007/s00162-007-0053-2.
- [3] Medina, A., SureshBabu, A., Rockwood, M. P., Gopalarathnam, A., and Anwar, A., "Theoretical and Experimental Study of Wake Encounters on Unsteady Airfoils," AIAA Paper 2019-0898, January 2019.
- [4] Ellington, C., "The aerodynamics of hovering insect flight," *Philos. Trans. R. Soc. B*, Vol. 305, 1984. https://doi.org/10.1098/rstb.1984.0049.
- [5] Dickinson, M. H., Lehmann, F. O., and Sane, S. P., "Wing Rotation and the Aerodynamic Basis of Insect Flight," *Science*, Vol. 284, No. 5422, 1999, pp. 1954–1960. https://doi.org/10.1126/science.284.5422.195.
- [6] Ellington, C., van den Berg, C., Willmott, A., and Thomas, A., "Leading-edge vortices in insect flight," *Nature*, Vol. 384, 1996. https://doi.org/10.1038/384626a0.
- [7] Pullin, D., and Wang, Z., "Unsteady forces on an accelerating plate and application to hovering insect flight," *J. Fluid Mech*, Vol. 509, 2004. https://doi.org/10.1017/S0022112004008821.
- [8] Eldredge, J. D., and Jones, A. R., "Leading-Edge Vortices: Mechanics and Modeling," *Annual Review of Fluid Mechanics*, Vol. 104, 2019. https://doi.org/10.1146/annurev-fluid-010518-040334.
- [9] Küssner, H. G., "Stresses produced in airplane wings by gusts," Tech. Rep. 645, NACA, 1932.
- [10] Gudmundsson, S., "Chapter 16 Performance Introduction," 2014, pp. 761–789. https://doi.org/10.1016/B978-0-12-397308-5.00016-7.
- [11] Hermann, B., Brunton, P. J. E., Steven L., and Semaan, R., "Gust mitigation through closed-loop control. II. Feedforward and feedback control," *Physical Review Fluids*, Vol. 7, 2022. https://doi.org/10.1103/PhysRevFluids.7.024706.
- [12] Corkery, B. H., S. J., and Harvey, J. K., "On the development and early observations from a towing tank-based transverse wing–gust encounter test rig," Vol. 59, No. 9, 2018, p. 135. https://doi.org/10.1007/s00348-018-2586-0.
- [13] Andreu-Angulo, B. H. B. H. S. G., I., and Jones, A. R., "Effect of transverse gust velocity profiles," Vol. 58, No. 12, 2020, p. 5123–5133. https://doi.org/10.2514/1.J059665.
- [14] Sedky, G., Gementzopoulos, A., Andreu-Angulo, I., Lagor, F. D., and Jones, A. R., "Physics of gust response mitigation in open-loop pitching manoeuvres," *Journal of Fluid Mechanics*, Vol. 944, 2022, p. A38. https://doi.org/10.1017/jfm.2022.509.

- [15] Wagner, H., "Über die Entstehung des dynamischen Auftriebes von Tragflügeln," ZAMM Journal of Applied Mathematics and Mechanics / Zeitschrift für Angewandte Mathematik und Mechanik, Vol. 5, No. 1, 1925, pp. 17–35. https://doi.org/10.1002/ zamm.19250050103.
- [16] Sedky, G., Lagor, F. D., and Jones, A., "Unsteady aerodynamics of lift regulation during a transverse gust encounter," *Physical Review Fluids*, Vol. 5, 2020, p. 074701. https://doi.org/10.1103/PhysRevFluids.5.074701.
- [17] Ramesh, K., Gopalarathnam, A., Granlund, K., Ol, M., and Edwards, J., "Discrete-Vortex Method with Novel Shedding Criterion for Unsteady Airfoil Flows with Intermittent Leading-Edge Vortex Shedding," *Journal of Fluid Mechanics*, Vol. 751, 2014, pp. 500–538. https://doi.org/10.1017/jfm.2014.297.
- [18] Narsipur, S., Gopalarathnam, A., and Edwards, J. R., "Low-Order Model for Prediction of Trailing-Edge Separation in Unsteady Flow," *AIAA Journal*, Vol. 57, No. 1, 2019, pp. 191–207. https://doi.org/10.2514/1.J057132.
- [19] Narsipur, S., Gopalarathnam, A., and Edwards, J. R., "Low-Order Modeling of Dynamic Stall on Airfoils in Incompressible Flow," *AIAA Journal*, 2022, pp. 1–17. https://doi.org/10.2514/1.J061595.
- [20] Narsipur, S., Hosangadi, P., Gopalarathnam, A., and Edwards, J. R., "Variation of Leading-Edge Suction during Stall for Unsteady Aerofoil Motions," *Journal of Fluid Mechanics*, Vol. 900, 2020. https://doi.org/10.1017/jfm.2020.467.
- [21] Saini, A., and Gopalarathnam, A., "Leading-Edge Flow Sensing for Aerodynamic Parameter Estimation," *AIAA Journal*, Vol. 56, No. 12, 2018, pp. 4706–4718. https://doi.org/10.2514/1.J057327.
- [22] Saini, A., Narsipur, S., and Gopalarathnam, A., "Leading-Edge Flow Sensing for Detection of Vortex Shedding from Airfoils in Unsteady Flows," *Physics of Fluids*, Vol. 33, No. 8, 2021, p. 087105. https://doi.org/10.1063/5.0060600.
- [23] SureshBabu, A., Ramesh, K., and Gopalarathnam, A., "Model Reduction in Discrete-Vortex Methods for Unsteady Airfoil Flows," *AIAA Journal*, Vol. 57, No. 4, 2019, pp. 1409–1422. https://doi.org/10.2514/1.J057458.
- [24] Lee, Y. T., SureshBabu, A., Bryant, M., and Gopalarathnam, A., "State Variable Form of Unsteady Airfoil Aerodynamics with Vortex Shedding," AIAA SCITECH 2022 Forum 2022-1667, 2022. https://doi.org/10.2514/6.2022-1667.
- [25] Leonard, A., "Vortex methods for flow simulation," Journal of Computational Physics, Vol. 37, No. 3, 1980, pp. 289–335. https://doi.org/https://doi.org/10.1016/0021-9991(80)90040-6.
- [26] Aggarwal, S., "An inviscid numerical method for unsteady flows over airfoils and wings to predict the onset of leading edge vortex formation,", 2017.
- [27] Suresh Babu, A. V., Narsipur, S., Bryant, M., and Gopalarathnam, A., "Leading-edge-vortex tailoring on unsteady airfoils using an inverse aerodynamic approach," *Physics of Fluids*, Vol. 34, No. 5, 2022. https://doi.org/10.1063/5.0090328.
- [28] Helmbold, H., "Der unverwundene ellipsenflugel als tragende flanche," Jahrbuch, 1942, pp. I111–I113.
- [29] Eldredge, J. D., and Wang, C., "Low-order phenomenological modeling of leading-edge vortex formation," *Theoretical and Computational Fluid Dynamics*, Vol. 27, 2013, pp. 577–598. https://doi.org/10.1007/s00162-012-0279-5.
- [30] Kenneth, G., Ol, M., and Bernal, L., "Experiments on Pitching Plates: Force and Flowfield Measurements at Low Reynolds Numbers," AIAA Paper 2011-0872, https://doi.org/10.2514/6.2011-872, 2011.